Research Square

Preprints are preliminary reports that have not undergone peer review. They should not be considered conclusive, used to inform clinical practice, or referenced by the media as validated information.

Three-Dimensional Walnut-Like, Hierarchically Zn-MOF Microsphere: One-Pot Synthesis, Characterization And Its Application as a Green Catalyst For The Asymmetric Hantzsch Synthesis of Polyhydroquinolines

Sayed Mohammad Ramish
Ilam University
Arash Ghorbani-Choghamarani (a.ghorbani@basu.ac.ir)
Bu-Ali Sina University
Masoud Mohammadi
Ilam University

Research Article

Keywords: Metal Organic Frameworks (MOF), Microspheres, Zn-MOF, Walnut-like, Hantzsch Reaction, Polyhydroquinolines

Posted Date: October 21st, 2021

DOI: https://doi.org/10.21203/rs.3.rs-955041/v1

License: This work is licensed under a Creative Commons Attribution 4.0 International License. Read Full License

Abstract

A three-dimensional walnut-like, microsphere Zn-based MOFs system was designed and synthesized *via* hydrothermal reaction of zinc salt with 4,6-diamino-2-pyrimidinethiol as a tridentate ligand. Besides, Zn ions were coordinated to the ligand's functional groups to give a novel Zn-MOF microsphere material. Afterward, the resultant material was thoroughly characterized by various analysis and physico-chemical methods; including, FT-IR, XRD, TGA, EDX, X-ray mapping, SEM, TEM, and BET analysis. The Zn-MOF microspheres were utilized in the Hantzsch reaction for selective synthesis of asymmetric polyhydroquinolines, using various aromatic aldehydes. Our strategy provides a way for controlled synthesis of the hierarchically nanoporous Zn-MOF microspheres with well-defined morphology, structure, and excellent catalytic properties, resulting in having a promising heterogeneous catalyst for a selective synthesis with good yields in the short reaction time and a low limit of steric hindrance and electronic effects. Besides, the heterogeneity of the catalyst is further tested with hot filtration and also the reusability results point.

1. Introduction

Porous materials with large specific surface areas and other unique properties have gained increasing attention [1]. During the last two decades, it has been revealed that Metal-organic frameworks (MOFs) have extensive applications in drugs delivery, absorption, and desorption of substances, biomedicines, and catalysis due to their desired morphology, high surface area, stability, active metal sites, and controllable pore size [2–7]. Among them, coordination polymer microspheres have drawn great attention for their potential applications in many fields especially in the catalytic synthesis of various organic and bioorganic molecules via organic transformations [8–11]. They can be regarded as a novel class of crystalline porous compounds formed by the strong bonding of metal ions or clusters to polytopic organic ligands, giving rise to extended networks [9, 12]. Since traditional microspheres have some drawbacks, i.e. higher product costs because of expensive excipients or sophisticated equipment and stricter quality control [13, 14], the nanoporous microspheres with low density and high specific surface area have become a pragmatic manner to address the existing problems [15–18].

Recently, some specific efforts have been made to design effective microsphere catalysts with external pores on the surface or internal pores in the core (which can be regarded as the main difference between porous microspheres and traditional microspheres), instead of using traditional microsphere catalysts based on expensive metals [1, 8, 19–23]. Besides, porosity is very significant in measuring the capacity efficiency of the catalysts. Moreover, the applied porous microspheres have been based on the porous structure, i.e. the amount, diameter, the structure of the pores, etc., which can be controlled by chemical and physical techniques [24, 25]. Among all of the transition metal-based catalysts used in organic transformations, Zinc has gained great attention due to its precious properties such as low cost, nontoxicity, good availability, and being ecofriendly. Therefore, many studies have shown the implementation of catalytic systems based on Zn using various linkers in organic reactions [26–31].

The asymmetric reaction of an aldehyde, two components of β-keto esters, and a nitrogen donor is known as Hantzsch method which generates chiral dihydropyridines. Besides, they have been regarded as useful precursors to many compounds of biological and pharmaceutical interest, i.e. different natural products [32]. When transition metal catalysts are present, Polyhydroquinolines with the functionalized aromatic rings can be generated from this reaction [33–36]. Among various catalysts developed so far, the efficiency of the catalytic systems is generally limited by their low yield, use of volatile organic solvents, harsh reaction condition, aggregation tendency as well as poor mechanical properties, high catalyst loading, tedious workup procedure, and separation of catalyst residue from the reaction mixture [32]. Although this method is practically useful for the synthesis of interesting pharmaceutical products, its selectivity and substrate scope still need to be improved [32, 37, 38]. We propose to develop a novel selective heterogeneous catalytic system for the recognition of the polyhydroquinoline derivatives to facilitate the screening of the catalysts for this asymmetric reaction.

In this work, we studied the hydrothermal synthesis of novel Zn-based nanoporous microspheres, by the reaction of zinc nitrate hexahydrate salt with 4,6-Diamino-2-pyrimidinethiol containing amine, thiol, and pyrimidine functional groups. We found out that Zn-MOFs can be used as a rapid catalyst for the synthesize the polyhydroquinolines with excellent yields. It represents a new method for the clean and rapid synthesis of asymmetric dihydropyridines. Herein, these results are reported.

2. Experimental

2.1. Materials

All reagents and solvents were purchased from Merck and used without additional purification.

2.2. Synthesis of nanoporous Zn-MOF microspheres

To prepare Zn-MOF porous microspheres, 4,6-Diamino-2-pyrimidinethiol (1 mmol) was dissolved in water (2 mL) and, then, it was added to a solution of DMF (12 mL) containing 2 mmol of $Zn(NO_3)_2.6H_2O$ salt through 20 minutes of stirring at 80 ºC until reaching a clear solution. Afterward, the white suspension was transferred into a Teflon lined autoclave reactor and heated at 160 ºC for 24 h (Scheme1), which then cooled to the room temperature at a gradient of 40°C per hour. Subsequently, the target Zn-MOF microsphere yellow powder was obtained after the sonication in ethyl acetate.

2.3. General procedure for the catalytic synthesis of polyhydroquinolines

A mixture of Substituted aromatic aldehyde (1.0 mmol) ethyl acetoacetate (1 mmol), and dimedone (1 mmol), were stirred with Ammonium acetate as a green NH_3 source (1.2 mmol), and Zn-MOF microspheres (8 mg) in PEG-400 (2 mL) for 70-180 min at 80°C. Completion of the following reaction has been analyzed via TLC. Subsequent to cooling at room temperature, the catalyst was separated using simple filtration and the resultant mixture's preparation was extracted using Ethyl acetate and water

derivation to gather unrefined polyhydroquinoline product, which was further purified through recrystallization in ethanol.

3. Results And Discussions

This study reports the synthesis of nanoporous Zn-MOF microspheres to develop an efficient and novel heterogeneous catalyst to synthesize polyhydroquinolines as an important dihydropyridine-containing scaffold via Hantzsch reaction. The resulting samples were characterized using various techniques.

3.1. Synthesis and characterization of the catalyst

The heterogeneous Zn-MOF microsphere catalyst was successfully prepared by hydrothermal reaction of $Zn(NO_3)_2.6H_2O$ and 4,6-Diamino-2-pyrimidinethiol, using the deprotonation of amine and thiol groups. Afterward, metal coordination bonding to the Zn ions was made to give a novel Zn-based microsphere catalyst. This newly synthesized nanoporous microsphere catalyst was fully characterized by various techniques; including, FT-IR, XRD, TGA, EDX, X-ray mapping, SEM, TEM and BET analysis. The results obtained from these techniques confirmed the successful preparation of this novel catalyst.

3.2. Structural and chemical composition analysis

The changes in the chemical features during the synthesis of the composite were measured by FT-IR, spectroscopy. Figure 1 shows the FT-IR spectra of a) 4,6-Diamino-2-pyrimidinethiol, b) $Zn(NO_3)_2.6H_2O$ and c) nanoporous Zn-MOF microspheres, respectively. In the FT-IR spectrum of the 4,6-Diamino-2-pyrimidinethiol (Figure. 1a), the bands at 3339 cm^{-1} and 3435 cm^{-1} are attributed to the stretching vibration of the N-H bonds of free NH_2 groups while those at 1523 cm^{-1} are related to the C=C group of the pyrimidine ring. The Amine bands disappeared in the FT-IR spectra of the Zn-MOF microspheres (Figure. 1c), which show that the NH_2 groups have been deprotonated and coordinated to the Zn atoms. Also, the bending vibration of NH_2 at 1638 cm^{-1} in the Zn-MOF microspheres shows a shift towards higher frequencies as compared to the primary sample. This shift can be assigned to the presence of Zn ions in MOF structure and the reduction of the single bond nature of the amine and thiol groups, which confirms the successful complexion of Zn ions with the N and S atoms in the framework. The strong C=C stretching vibration band at 1468 cm^{-1} and C-N stretch band at 1102 cm^{-1} provide shreds of evidence confirming the successful synthesis of the final MOF (Figure. 1c).

The crystalline phases of nanoporous Zn-MOF microspheres were examined by X-ray diffraction (XRD) analysis as shown in Fig. 2. The characteristic diffraction peaks corresponding to the obtained framework are found at 2θ = 31.62 °, 34.49 °, 36.15 °, 47.42 °, 56.3 °, 62.57 °, 67.75 °, 68.95 °, 72.51 ° and 76.82 ° which effectively coincide with XRD patterns simulated from powder X-ray data of nanoporous Zn-MOF microspheres with a cubic phase [39–41]. Based on the XRD results, we can also observe that the Zn-MOF microspheres obtained from zinc nitrate show sharp characteristic peaks, suggesting the high crystalline nature of the obtained nanoporous Zn-MOF microspheres.

To estimate the mass ratios and the thermal stability of nanoporous Zn-MOF microspheres, the TGA-DSC technique was employed. Fig. 3. represents TGA (Maroon line) and DSC (Blue line) curves of Zn-MOF microspheres at the temperature range of 25-1500 ℃. In the TGA curve, the weight loss which was occurred below 200°C was attributed to the release of the physically adsorbed moisture and water and organic solvents from the sample [42]. The next weight loss (10.61%) in the region of 200-800 ℃ can be associated with the decomposition of 4,6-Diamino-2-pyrimidinethiol ligand [43, 44]. In addition, the weight loss at 450 ℃ indicates the decomposition of the framework. A basic point about the nature of the Zn-MOF catalyst is the thermal stability of the catalyst up to 200 ℃; therefore, this catalyst can be used under various catalytic reaction conditions up to 200 ℃.

As shown in figure 4, energy dispersive X-ray (EDX) analysis was applied to determine the chemical composition of nanoporous Zn-MOF microspheres. The results indicate the presence of 53.25 W% of Zn species in the obtained nanoporous Zn-MOF microsphere catalyst. In addition, the presence of carbon (10.70 W%), nitrogen (9.11 W%) sulfur (13.97 W%) and oxygen (12.97 W%) elements in the prepared nanoporous material was also confirmed by these measurements. These observations support the high purity of the prepared Zn-MOF microspheres.

The uniform distribution of the index elements (C, S, N, O, and Zn) of the obtained nanoporous material is observed at the X-ray mapping analysis (Fig. 5). In addition, the uniform distribution of the Zn element shows that it has evenly coordinated to N and S elements, indicating the presence of ligand in the obtained frameworks, and the uniform incorporation of the activated Zn catalytic species with S and N groups showing that an excellent catalytic surface has been formed.

The surface morphology of the prepared nanoporous material was assessed by scanning electron microscopy (FE-SEM) and transmission electron microscopy (TEM) analysis. The FE-SEM images for pure nanoporous Zn-MOF microspheres are presented in Fig. 6. A closer look at the SEM images of the obtained nanoporous material indicates that the Zn-MOF has been formed in uniform three-dimensional walnut-like hierarchically nanoporous microparticle morphology, which can be attributed to a proper bonding in-between the metal and linker. Moreover, the SEM images show that these Zn-MOF microparticles are composed of a collection of nanoparticles having a mean particle size of 23-27 nm. The results indicate that the Zn-MOF microspheres have been formed in a uniform manner. Besides, there is no indication of agglomeration of the particles and also this feature optimizes the catalytic properties of the samples.

By applying the transmission electron microscopy technique, high-quality images from the synthesized crystalline nanoporous Zn-MOF microspheres were obtained (Figure 7). As can be seen, the synthesized Zn-MOF microspheres exhibit characteristic yolk-shell structure and a clear gap existed between the shell and the core, confirming that the core is a solid sphere. Particle size distribution histogram of the as-prepared microspheres gave distribution dimensions across a range from 90 to 170 nm, with an average size of 130 nm (Figure 7).

The porosity and surface characteristics of nanoporous Zn-MOF microspheres were explored by the N_2 adsorption/desorption analysis (Fig. 8). The obtained results are illustrated in Figure 8. Zn-MOF microspheres exhibited a Brunauer–Emmett–Teller (BET) surface area of 63.33 $m^2.g^{-1}$ and the pore volumes and pore size distribution of nanoporous Zn-MOF microspheres are calculated by BJH analysis, as the values are 0.088 $cm^3.g^{-1}$, and 1.22 nm, respectively.

4. Catalytic Study

After the successful characterization of the synthesized Zn-MOF microsphere, We applied these nanoporous materials as a novel catalyst for the multicomponent synthesis of polyhydroquinolines under diverse conditions (Table 1). We optimized conditions of the reaction for Hantzsch synthesis of dihydropyridine scaffolds using *para*-chlorobenzaldehyde, dimedone, ethyl acetoacetate, and ammonium acetate as a model reaction. Afterward, various parameters of the reaction, including the amount of catalyst, solvent, and temperature, were evaluated for the model reaction, the results of which are summarized in Table 1. When there is no catalyst in the reaction, no reaction takes place (Table 1, entry 1). In this sense, it is worth mentioning that the existence of Zn-MOF microsphere is required for this type of Hantzsch reaction. The reaction proceeds faster by increasing the catalyst amount up to 10 mg. According to the results, 10 mg of the catalyst is required for the reaction. Using smaller amounts of the catalyst will cause the reaction to be incomplete (Table 1, entry 4 & 5). Increasing the amount of catalyst by more than 10 mg does not affect the efficiency percentage (Table 1, entry 7). Additionally, the catalytic effect of 4,6-diamino-2-pyrimidinethiol and $Zn(NO_3)_2.6H_2O$ was investigated on the model reaction. It was observed that they cannot efficiently catalyze the reaction and, as a result, the product is obtained in low yields in 85 min. Among the various solvents used in the reaction, the results indicate that the PEG-400 as a solvent which showed a higher efficiency, as compared to all solvents tested with 96% isolated yield, may serve as both the solvent and the phase transfer catalyst in this type of reaction (Table 1, entry 6). Finally, the reaction was performed at different temperatures, and the low temperature continued with lower efficiency (Table 1, entry 6, 12-14). Regarding the optimization studies, the optimum conditions for this reaction are 10 mg of Zn-MOF in the PEG-400 at 80°C (Table 1, entry 6).

Table 1
Optimization of the reaction conditions for the Hantzsch condensation of *para*-Chlorobenzaldehyde, dimedone, ethyl acetoacetate, and ammonium acetate as a model reaction for the synthesis of polyhydroquinolines.

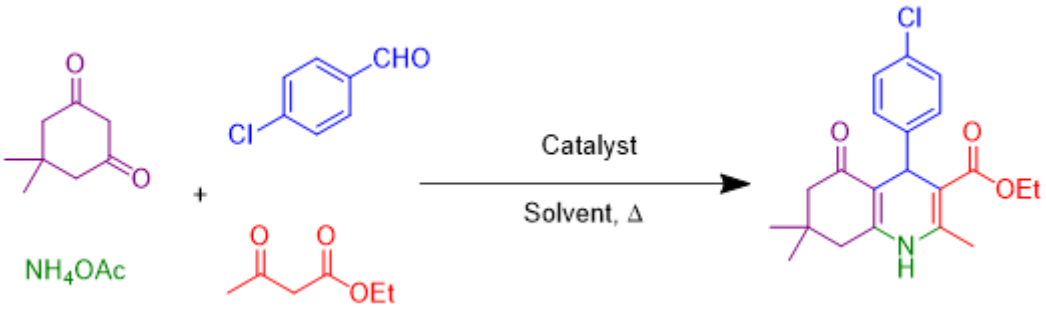

Entry	**Catalyst**	**Amount Catalyst (mg)**	**Solvent**	**Temperature (ºC)**	**Time (min)**	**Yield (%)[a,b]**
1	-	-	PEG-400	80	85	30
2	4,6-diamino-2-pyrimidinethiol	10	PEG-400	80	85	41
3	$Zn(NO_3)_2.6H_2O$	10	PEG-400	80	85	30
4	Zn-MOF	5	PEG-400	80	85	75
5	Zn-MOF	6	PEG-400	80	85	79
6	Zn-MOF	10	PEG-400	80	85	96
7	Zn-MOF	12	PEG-400	80	85	92
8	Zn-MOF	10	EtOH	80	195	83
9	Zn-MOF	10	H_2O	80	120	N.R
10	Zn-MOF	10	DMF	80	210	60
11	Zn-MOF	10	DMSO	80	95	70
12	Zn-MOF	10	PEG-400	25	120	N.R

[a] Isolated yield.

[b] Reaction conditions: 4-Chlorobenzaldehyde (1mmol), dimedone (1 mmol), ethyl acetoacetate (1 mmol), ammonium acetate (1.2 mmol), catalyst (mg) and solvent (2mL).

13	Zn-MOF	10	PEG-400	60	85	21
14	Zn-MOF	10	PEG-400	100	85	44

[a] Isolated yield.

[b] Reaction conditions: 4-Chlorobenzaldehyde (1mmol), dimedone (1 mmol), ethyl acetoacetate (1 mmol), ammonium acetate (1.2 mmol), catalyst (mg) and solvent (2mL).

After optimizing the reaction conditions, we explored the scope of the reaction with various electron-donating and electron-withdrawing groups of aldehydes. In all cases, the products were made in high yields (Table 2). Although the results indicate that ortho and/or meta-substituted aryl aldehydes react slowly, as compared to the para isomers, electron-releasing and electron-withdrawing groups give an excellent yield of product.

Table 2 Hantzsch synthesis of polyhydroquinoline derivatives in the presence of Zn-MOF in PEG-400 at 80 °C.

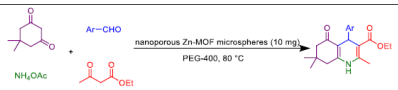

Entry	Aryl aldehyde	Product	Time (min)	Yield (%)[a,b]	Melting point	
					measured	literature
1		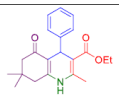	150	83	216-218	217-219 [45]
2		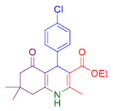	85	96	237-240	234-237 [45]
3		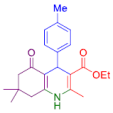	120	74	252-255	252-255 [46]
4		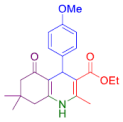	70	58	247-250	245-247 [46]
5		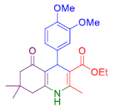	180	69	201-204	203-204 [45]
6		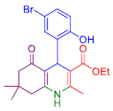	150	79	263-265	246 – 248 [45]
7		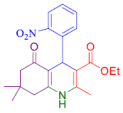	75	95	173-175	176-178 [45]
8		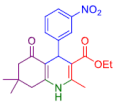	90	85	217-219	216-218 [45]
9		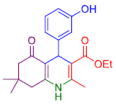	90	97	217-219	216-218 [45]
10		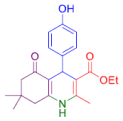	150	92	227-229	231–233 [46]
11		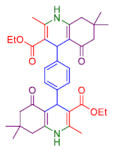	90	91	301-303	303-305 [45]

[b] Isolated yields.

[b] Reaction conditions: Aromatic aldehyde (1mmol), dimedone (1 mmol), ethyl acetoacetate (1 mmol), ammonium acetate (1.2 mmol), Zn-MOF (10 mg) and PEG-400 (2mL) at 80°C.

[c] Reaction conditions: Aromatic aldehyde (1mmol), dimedone (2 mmol), ethyl acetoacetate (2 mmol), ammonium acetate (2.4 mmol), Zn-MOF (20 mg) and PEG-400 (4 mL) at 80°C.

It is worth noting that an appropriate mechanism for the polyhydroquinoline derivatives' synthesis reaction, catalyzed by nanoporous Zn-MOF microspheres, was proposed (Scheme 2) [32]. Firstly, the reaction was granted to start through deprotonation of the dimedone which underwent Knoevenagel condensation reaction with an aldehyde to form an α,β-unsaturated compound. Subsequently, the Michael addition of imine (which was achieved from the combination of NH_3 with ethyl acetoacetate) on the α,β-unsaturated carbonyl compounds, followed by cyclization reaction, generated a six-membered ring. Finally, the dehydration gave the final polyhydroquinoline products (Scheme 2) [32].

5. Catalyst Reusability Studies:

Recyclability of the heterogeneous catalyst put an end to the use of harmful and costly metal catalysts while decreasing the cost of products. These factors are of crucial importance from an economical point of view. Recyclability of the nanoporous Zn-MOF microsphere was investigated in the model reaction. The catalyst was separated after completion of the reaction, washed with ethyl acetate and acetone and, then, dried at 70°C. The dried catalyst was reused for the next cycle. The recycled catalyst was employed in the four sequential cycles; the yield of the reaction was decreased moderately after the fourth run of the reaction, as illustrated in Fig. 9.

6. Hot Filtration

The hot filtration test was another analysis to approve the heterogeneous nature of the nanoporous Zn-MOF microspheres in the Hantzsch synthesis of polyhydroquinolines. On this basis, the model reaction was studied again under the optimized reaction condition. After 43 min (59 % conversion), the Zn-MOF was removed from the reaction by simple filtration. Afterward, the rest of the reaction was stirred in the absence of the catalyst for a further 43 min. The obtained results show that the Zn-based MOF played a catalytic role in the reaction without the Zn leaching into the solution or framework degradation.

7. Comparison

In the last part of our studies, to demonstrate the profit of nanoporous Zn-MOF microspheres as a heterogeneous catalyst in Hantzsch reaction, our resultant and reaction conditions were compared with those of the reported acid, base, and metal catalysts in the synthesis of polyhydroquinolines (Table 3). As depicted in Table 3, the nanoporous Zn-MOF microspheres are the most efficient catalysts to synthesize polyhydroquinolines. Significantly, most of the reported methods toil from the absence of commonness for the condensation reactions of the deactivated aldehydes. In addition, the reported synthetic paths have some limitations, such as requiring extreme temperature or long duration, large amounts of the catalyst, and most importantly, the use of hazardous solvents to give excellent yields. Promising results obtained in the presence of Zn-MOF microspheres should be ascribed to the nanoporous structure of the catalyst. The two roles of PEG-400 (solvent and phase transfer catalyst) avouch the better contact between the catalyst and the reactants and, thus, substantially raising the catalytic activity and stability of the catalyst.

Table 3
Comparison of the synthesis of polyhydroquinolines in the presence of various catalysts.

Entry	Catalyst	Time (min)	Yield (%)[a]	Ref
1	$FeAl_2O_4$	180	90	[47]
2	Fe_3O_4@D-NH-$(CH_2)_4$-SO_3H	90	86	[48]
3	Fe_3O_4@FSM-16-SO_3H	25	86	[49]
4	Fe_3O_4-TEDETA-Br_3	120	92	[50]
5	Fe_3O_4@SiO_2@$(CH_2)_3$Im}$C(NO_2)_3$	18	89	[51]
6	Fe_3O_4@SiO_2–PEG/NH_2	20	96	[52]
7	Fe_3O_4@GA@IG	45	89	[36]
8	AIL-SCMNPs	15	80	[53]
9	Zn-MOF	85	96	This work

[a] Isolated yield.

8. Conclusion

In conclusion, we have reported an efficient and novel three-dimensional walnut-like, nanoporous Zn-MOF microsphere catalytic system by hydrothermal method. It was able to accelerate the asymmetric Hantzsch reaction with various aryl aldehydes including electron-donor and electron-acceptor groups for in situ production of polyhydroquinolines. The present protocol gives an excellent yield of the product within a short reaction time, by easy workup and no need for further purification of the product. The novelty, simple synthesis procedure, no use of harmful solvents, facile filtration, high yield, and, especially, reusability are some of the advantages of the developed catalyst.

Declarations

Conflicts of interest

There are no conflicts of interest with this research work.

Acknowledgments

This work was supported by the research facilities of Ilam University, Ilam, Iran, and Bu-Ali Sina University, Hamedan, Iran.

References

1. Xu, J. *et al.* Three-Dimensional Walnut-Like, Hierarchically Nanoporous Carbon Microspheres: One-Pot Synthesis, Activation, and Supercapacitive Performance. *ACS Sustain. Chem. Eng*, **8**, 8024–8036 https://doi.org/10.1021/acssuschemeng.0c02677 (2020).
2. Yu, D. *et al.* A solvent-assisted ligand exchange approach enables metal-organic frameworks with diverse and complex architectures. *Nat. Commun*, **11**, 927 https://doi.org/10.1038/s41467-020-14671-9 (2020).
3. Ahmad, N. *et al.* Development of Mixed metal Metal-organic polyhedra networks, colloids, and MOFs and their Pharmacokinetic applications. *Sci. Rep*, **7**, 832 https://doi.org/10.1038/s41598-017-00733-4 (2017).
4. Supercapacitor made from MOF. *Nature*, **538**, 143 https://doi.org/10.1038/538143e (2016).
5. Li, T., Bai, Y., Wang, Y., Xu, H. & Jin, H. Advances in transition-metal (Zn, Mn, Cu)-based MOFs and their derivatives for anode of lithium-ion batteries. *Coord. Chem. Rev*, **410**, https://doi.org/10.1016/j.ccr.2020.213221 (2020).
6. Mohamed, N. A. *et al.* Studies on metal–organic framework (MOF) nanomedicine preparations of sildenafil for the future treatment of pulmonary arterial hypertension. *Sci. Rep*, **11**, 4336 https://doi.org/10.1038/s41598-021-83423-6 (2021).
7. Su, Y. S. *et al.* Dipolar order in an amphidynamic crystalline metal–organic framework through reorienting linkers. *Nat. Chem*, **13**, 278–283 https://doi.org/10.1038/s41557-020-00618-6 (2021).
8. Rogowski, L. W. *et al.* Symmetry breaking propulsion of magnetic microspheres in nonlinearly viscoelastic fluids. *Nat. Commun*, **12**, 1116 https://doi.org/10.1038/s41467-021-21322-0 (2021).
9. Hu, Y. *et al.* Bis(zinc(II)-dipicolylamine)-functionalized sub-2 μm core-shell microspheres for the analysis of N-phosphoproteome. *Nat. Commun*, **11**, 6226 https://doi.org/10.1038/s41467-020-20026-1 (2020).
10. Ding, Y. *et al.* Preparation of Hollow Cu and CuOx Microspheres with a Hierarchical Structure for Heterogeneous Catalysis. *ACS Appl. Mater. Interfaces*, **10**, 41793–41801 https://doi.org/10.1021/acsami.8b16246 (2018).
11. Feng, Y. *et al.* Sea-Urchin-like Hollow CuMoO4–CoMoO4 Hybrid Microspheres, a Noble-Metal-like Robust Catalyst for the Fast Hydrogen Production from Ammonia Borane. *ACS Appl. Energy Mater*, **4**, 633–642 https://doi.org/10.1021/acsaem.0c02521 (2021).
12. Wu, J. *et al.* One-step preparation and characterization of silk nano- and microspheres. *Polym. J*, **52**, 1395–1400 https://doi.org/10.1038/s41428-020-0392-z (2020).
13. https://doi.org/10.1016/j.ijpharm.2018.06.015.
14. Kumar, G. P. & Anand, J. Porous floating microspheres: A new dimension in controlled drug delivery, Res. J. Pharm. Technol. 4(2011) 1340–1357. https://www.scopus.com/inward/record.uri?eid=2-s2.0-84860369641&partnerID=40&md5=d71fd2298983ce814f3a427dc57c0f26.

15. Molvinger, K., Quignard, F., Brunel, D., Boissière, M. & Devoisselle, J. M. Porous Chitosan-Silica Hybrid Microspheres as a Potential Catalyst. *Chem. Mater*, **16**, 3367–3372 https://doi.org/10.1021/cm0353299 (2004).
16. Ahmed, A., Skinley, K., Herodotou, S. & Zhang, H. Core–shell microspheres with porous nanostructured shells for liquid chromatography. *J. Sep. Sci*, **41**, 99–124 https://doi.org/10.1002/jssc.201700850 (2018).
17. He, J. H., Xu, L., Wu, Y. & Liu, Y. Mathematical models for continuous electrospun nanofibers and electrospun nanoporous microspheres. *Polym. Int*, **56**, 1323–1329 https://doi.org/10.1002/pi.2370 (2007).
18. Na, X., Zhou, W., Li, J., Su, Z. & Ma, G. Preparation and Application of Porous Polymer Microspheres in Virus-Like Particles Purification. *Prog. Chem*, **30**, 5–13 https://doi.org/10.7536/PC170922 (2018).
19. Xu, J. *et al.* One-Stage Synthesis of Cagelike Porous Polymeric Microspheres and Application as Catalyst Scaffold of Pd Nanoparticles. *Macromolecules*, **44**, 3730–3738 https://doi.org/10.1021/ma200320a (2011).
20. Hamaloğlu, K. Ã. *et al.* Monodisperse-porous cerium oxide microspheres carrying iridium oxide nanoparticles as a heterogeneous catalyst for water oxidation. *Appl. Surf. Sci*, **547**, https://doi.org/10.1016/j.apsusc.2021.149219 (2021).
21. Yang, S. *et al.* Zinc-iron bimetallic-nitrogen doped porous carbon microspheres as efficient oxygen reduction electrocatalyst for zinc-air batteries. *Appl. Surf. Sci*, 546 https://doi.org/10.1016/j.apsusc.2021.148934 (2021).
22. Wang, T., Cui, G., Zhao, Y., Nurpeissova, A. & Bakenov, Z. Porous carbon nanotubes microspheres decorated with strong catalyst cobalt nanoparticles as an effective sulfur host for lithium-sulfur battery. *J. Alloys Compd*, **853**, https://doi.org/10.1016/j.jallcom.2020.157268 (2021).
23. Hamaloğlu, K. Ã. *et al.* Monodisperse-porous cerium oxide microspheres as a new support with appreciable catalytic activity for a composite catalyst in benzyl alcohol oxidation. *New J. Chem*, **45**, 2019–2029 https://doi.org/10.1039/d0nj05367h (2021).
24. Hasani, A. *et al.* Recent progress of two-dimensional materials and metal–organic framework-based taste sensors. *J. Korean Ceram. Soc*, **57**, 353–367 https://doi.org/10.1007/s43207-020-00047-8 (2020).
25. Chen, D., Wei, L., Li, J. & Wu, Q. Nanoporous materials derived from metal-organic framework for supercapacitor application. *J. Energy Storage*, **30**, https://doi.org/10.1016/j.est.2020.101525 (2020).
26. Gong, Y., Zhu, Z., Qian, Q., Tong, W. & Gong, H. Zn- And Cu-catalyzed coupling of tertiary alkyl bromides and oxalates to forge challenging C–O, C–S, and C–N bonds. *Org. Lett*, **23**, 1005–1010 https://doi.org/10.1021/acs.orglett.0c04206 (2021).
27. Shen, H. M. *et al.* Efficient oxidation of cycloalkanes with simultaneously increased conversion and selectivity using O2 catalyzed by metalloporphyrins and boosted by Zn(AcO)2: A practical strategy to inhibit the formation of aliphatic diacids. *Appl. Catal. A Gen*, **609**, 117904 https://doi.org/10.1016/j.apcata.2020.117904 (2021).

28. Trost, B. M. & Zhu, C. Zn-ProPhenol Catalyzed Enantioselective Mannich Reaction of 2 H-Azirines with Alkynyl Ketones. *Org. Lett*, **22**, 9683–9687 https://doi.org/10.1021/acs.orglett.0c03737 (2020).
29. Yuan, Y. *et al.* Synthesis of Aza-Eight-Membered Ring-Fused Indolines Initiated by Zn-Catalyzed C2 Alkylation of Indoles and Subsequent Base-Promoted Ring Expansion. *Org. Lett*, **22**, 6532–6536 https://doi.org/10.1021/acs.orglett.0c02307 (2020).
30. Trost, B. M. *et al.* Direct Enantio- and Diastereoselective Zn-ProPhenol-Catalyzed Mannich Reactions of CF 3 - and SCF 3 -Substituted Ketones. *Org. Lett*, **22**, 2437–2441 https://doi.org/10.1021/acs.orglett.0c00646 (2020).
31. Mohammadi, M., Khodamorady, M., Tahmasbi, B., Bahrami, K. & Ghorbani-Choghamarani, A. Boehmite nanoparticles as versatile support for organic–inorganic hybrid materials: Synthesis, functionalization, and applications in eco-friendly catalysis. *J. Ind. Eng. Chem*, https://doi.org/10.1016/j.jiec.2021.02.001 (2021).
32. Kazemi, M. & Mohammadi, M. Magnetically Recoverable Catalysts: Catalysis in Synthesis of Polyhydroquinolines. *Appl. Organomet. Chem*, **34**, e5400 https://doi.org/10.1002/aoc.5400 (2020).
33. Rathee, G., Kohli, S., Singh, N., Awasthi, A. & Chandra, R. Calcined Layered Double Hydroxides: Catalysts for Xanthene, 1,4-Dihydropyridine, and Polyhydroquinoline Derivative Synthesis. *ACS Omega*, **5**, 15673–15680 https://doi.org/10.1021/acsomega.0c01901 (2020).
34. Rathee, G. *et al.* Fabrication of a Gold-Supported NiAlTi-Layered Double Hydroxide Nanocatalyst for Organic Transformations. *ACS Omega*, **5**, 23967–23974 https://doi.org/10.1021/acsomega.0c03250 (2020).
35. Sashidhara, K. V. *et al.* Discovery of Coumarin–Dihydropyridine Hybrids as Bone Anabolic Agents. *J. Med. Chem*, **56**, 109–122 https://doi.org/10.1021/jm301281e (2013).
36. Pourian, E., Javanshir, S., Dolatkhah, Z., Molaei, S. & Maleki, A. Ultrasonic-Assisted Preparation, Characterization, and Use of Novel Biocompatible Core/Shell Fe3O4@GA@Isinglass in the Synthesis of 1,4-Dihydropyridine and 4 H-Pyran Derivatives, ACS Omega. 3 (2018)5012–5020. https://doi.org/10.1021/acsomega.8b00379.
37. Sam, M., Dekamin, M. G. & Alirezvani, Z. Dendrons containing boric acid and 1,3,5-tris(2-hydroxyethyl)isocyanurate covalently attached to silica-coated magnetite for the expeditious synthesis of Hantzsch esters. *Sci. Rep*, **11**, 2399 https://doi.org/10.1038/s41598-020-80884-z (2021).
38. Moavi, J., Buazar, F. & Sayahi, M. H. Algal magnetic nickel oxide nanocatalyst in accelerated synthesis of pyridopyrimidine derivatives. *Sci. Rep*, **11**, 6296 https://doi.org/10.1038/s41598-021-85832-z (2021).
39. Salarian, M., Ghanbarpour, A., Behbahani, M., Bagheri, S. & Bagheri, A. A metal-organic framework sustained by a nanosized Ag12 cuboctahedral node for solid-phase extraction of ultra traces of lead(II) ions. *Microchim. Acta*, **181**, 999–1007 https://doi.org/10.1007/s00604-014-1200-2 (2014).
40. Ahmed, N. *et al.* Synthesis and characterization of Zn/ZnO microspheres on indented sites of silicon substrate. *Mater. Sci*, **36**, 501–508 https://doi.org/10.2478/msp-2018-0058 (2018).

41. Rajapriya, M. *et al.* Correction to: Synthesis and Characterization of Zinc Oxide Nanoparticles Using Cynara scolymus Leaves: Enhanced Hemolytic, Antimicrobial, Antiproliferative, and Photocatalytic Activity. *J. Clust. Sci*, **31**, 803–803 https://doi.org/10.1007/s10876-019-01734-1 (2020).
42. Maleki, B., Reiser, O., Esmaeilnezhad, E. & Choi, H. J. SO3H-dendrimer functionalized magnetic nanoparticles (Fe3O4@D–NH–(CH2)4–SO3H): Synthesis, characterization and its application as a novel and heterogeneous catalyst for the one-pot synthesis of polyfunctionalized pyrans and polyhydroquinolines. *Polyhedron*, **162**, 129–141 https://doi.org/10.1016/j.poly.2019.01.055 (2019).
43. Moradi, L. & Tadayon, M. Green synthesis of 3,4-dihydropyrimidinones using nano Fe3O4@meglumine sulfonic acid as a new efficient solid acid catalyst under microwave irradiation. *J. Saudi Chem. Soc*, **22**, 66–75 https://doi.org/10.1016/j.jscs.2017.07.004 (2018).
44. Ahmadi, A., Sedaghat, T., Azadi, R. & Motamedi, H. Magnetic Mesoporous Silica Nanocomposite Functionalized with Palladium Schiff Base Complex: Synthesis, Characterization, Catalytic Efficacy in the Suzuki–Miyaura Reaction and α-Amylase Immobilization. *Catal. Letters*, **150**, 112–126 https://doi.org/10.1007/s10562-019-02913-5 (2020).
45. Amoozadeh, A., Rahmani, S., Bitaraf, M., Abadi, F. B. & Tabrizian, E. Nano-zirconia as an excellent nano support for immobilization of sulfonic acid: a new, efficient and highly recyclable heterogeneous solid acid nanocatalyst for multicomponent reactions. *New J. Chem*, **40**, 770–780 https://doi.org/10.1039/C5NJ02430G (2016).
46. Ghorbani-Choghamarani, A., Mohammadi, M., Tamoradi, T. & Ghadermazi, M. Covalent immobilization of Co complex on the surface of SBA-15: Green, novel and efficient catalyst for the oxidation of sulfides and synthesis of polyhydroquinoline derivatives in green condition. *Polyhedron*, **158**, 25–35 https://doi.org/10.1016/j.poly.2018.10.054 (2019).
47. Ghorbani-Choghamarani, A., Mohammadi, M., Shiri, L. & Taherinia, Z. Synthesis and characterization of spinel FeAl2O4 (hercynite) magnetic nanoparticles and their application in multicomponent reactions. *Res. Chem. Intermed*, **45**, 5705–5723 https://doi.org/10.1007/s11164-019-03930-0 (2019).
48. Alinezhad, H., Tarahomi, M., Maleki, B. & Amiri, A. SO 3 H-functionalized nano-MGO-D-NH 2: Synthesis, characterization and application for one-pot synthesis of pyrano[2,3-d]pyrimidinone and tetrahydrobenzo[b]pyran derivatives in aqueous media. *Appl. Organomet. Chem*, 33 https://doi.org/10.1002/aoc.4661 (2019).
49. Hashemi-Uderji, S., Abdollahi-Alibeik, M. & Ranjbar-Karimi, R. Fe 3 O 4 @FSM-16-SO 3 H as a novel magnetically recoverable nanostructured catalyst: preparation, characterization and catalytic application. *J. Porous Mater*, **26**, 467–480 https://doi.org/10.1007/s10934-018-0628-x (2019).
50. Hajjami, M. & Gholamian, F. Tribromide ion immobilized on magnetic nanoparticle as a new, efficient and reusable nanocatalyst in multicomponent reactions. *RSC Adv*, **6**, 87950–87960 https://doi.org/10.1039/c6ra15474c (2016).
51. Yarie, M. *et al.* Novel magnetic nanoparticles with ionic liquid tags as a reusable catalyst in the synthesis of polyhydroquinolines. *RSC Adv*, **6**, 82842–82853 https://doi.org/10.1039/c6ra16459e

(2016).

52. Kardooni, R., Kiasat, A. R. & Motamedi, H. Designing of a novel dual-function silica-iron oxide hybrid based nanocomposite, Fe3O4@SiO2[sbnd]PEG/NH2, and its application as an eco-catalyst for the solvent-free synthesis of polyhydroacridines and polyhydroquinolines. *J. Taiwan Inst. Chem. Eng*, **81**, 373–382 https://doi.org/10.1016/j.jtice.2017.10.013 (2017).
53. Taheri, N., Heidarizadeh, F. & Kiasat, A. A new magnetically recoverable catalyst promoting the synthesis of 1,4-dihydropyridine and polyhydroquinoline derivatives via the Hantzsch condensation under solvent-free conditions. *J. Magn. Magn. Mater*, **428**, 481–487 https://doi.org/10.1016/j.jmmm.2016.09.099 (2017).

Figures

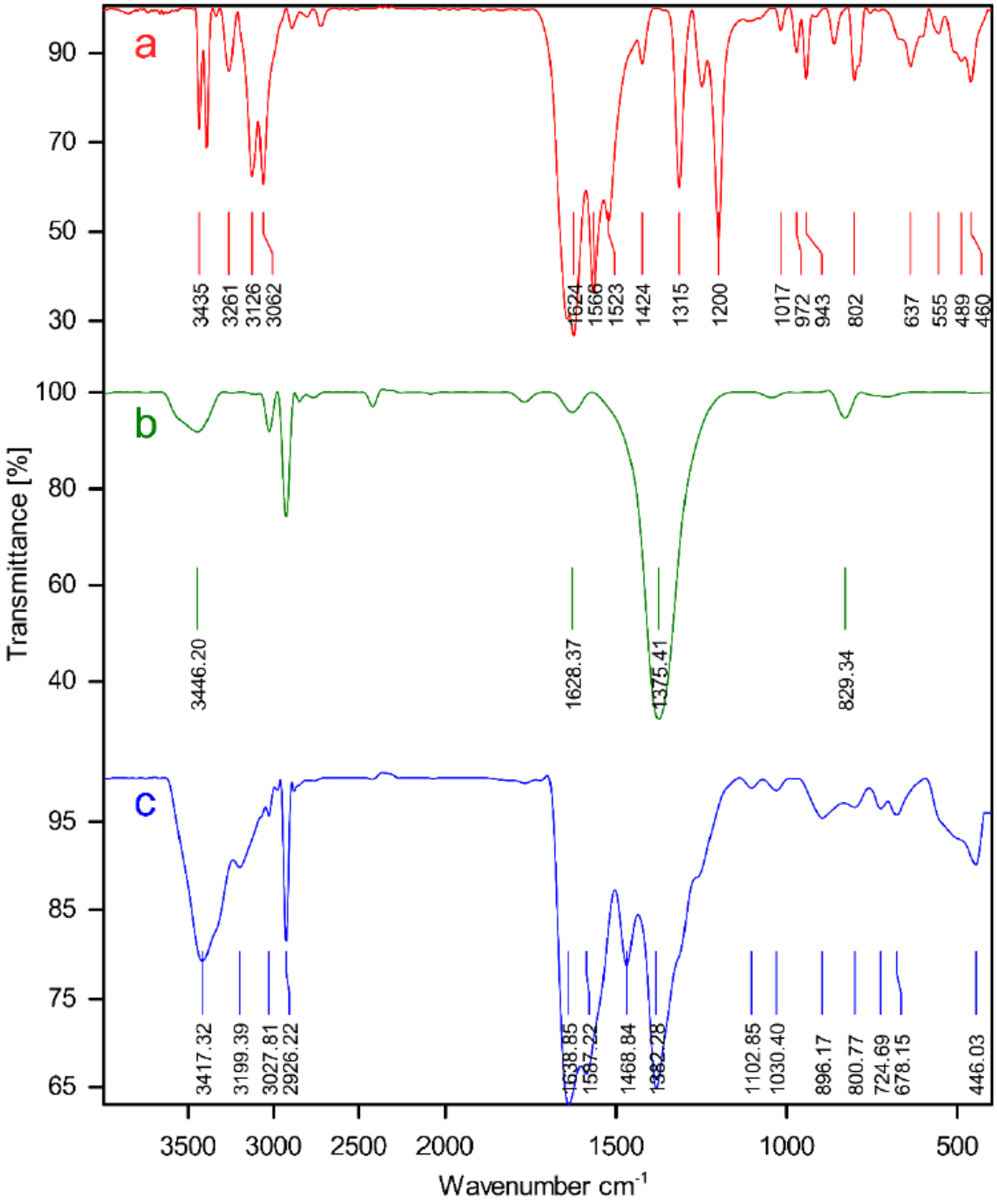

Figure 1

FT-IR Spectrums of a) 4,6-Diamino-2-pyrimidinethiol, b) Zn(NO3)2.6H2O and c) nanoporous Zn-MOF microspheres.

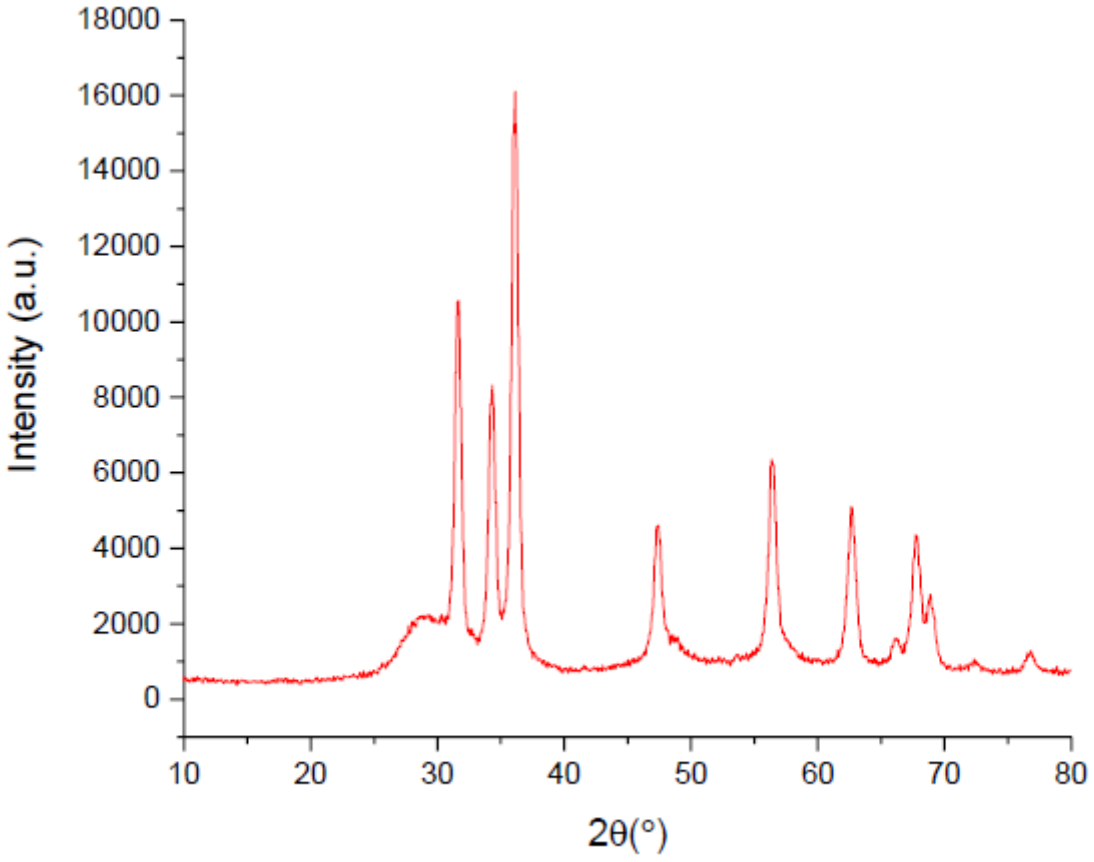

Figure 2

XRD pattern of nanoporous Zn-MOF microspheres.

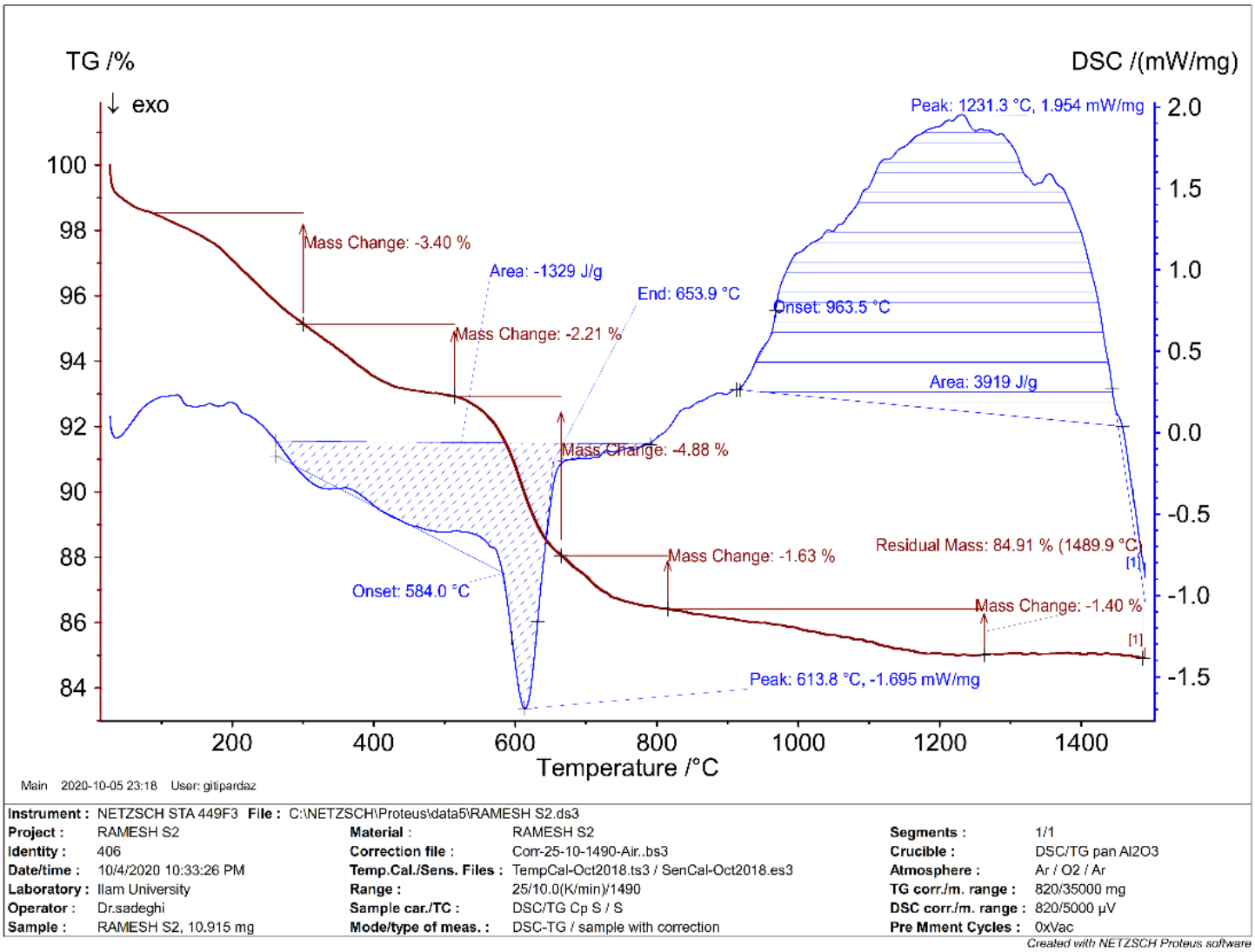

Figure 3

TGA (Maroon line) and DSC (Blue line) curves of nanoporous Zn-MOF microspheres.

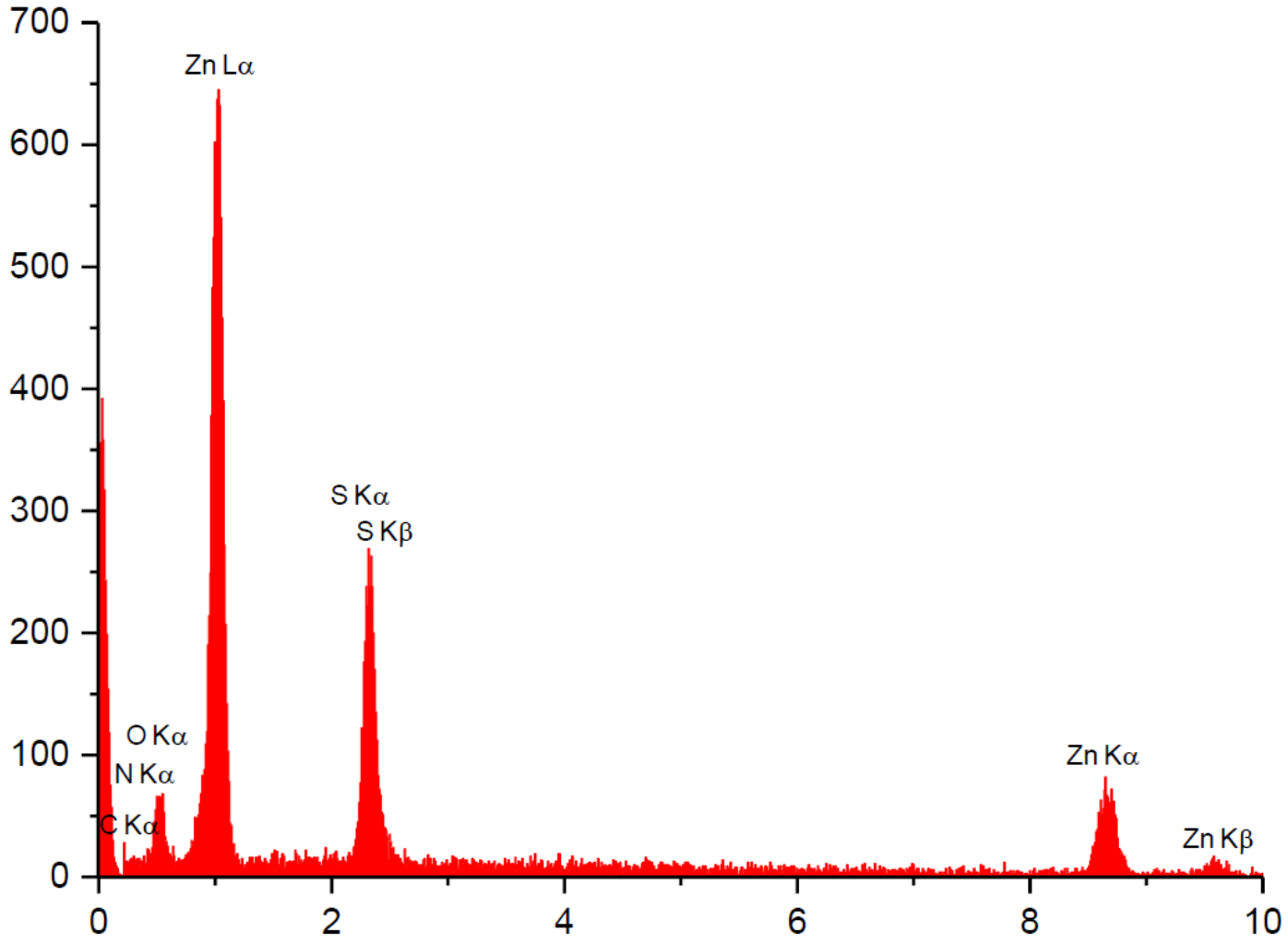

Figure 4

EDX Analysis of nanoporous Zn-MOF microspheres.

Figure 5

X-ray mapping Analysis of Zn-CA-CPS.

Figure 6

SEM images of three-dimensional walnut-like, hierarchically nanoporous Zn-MOF microspheres.

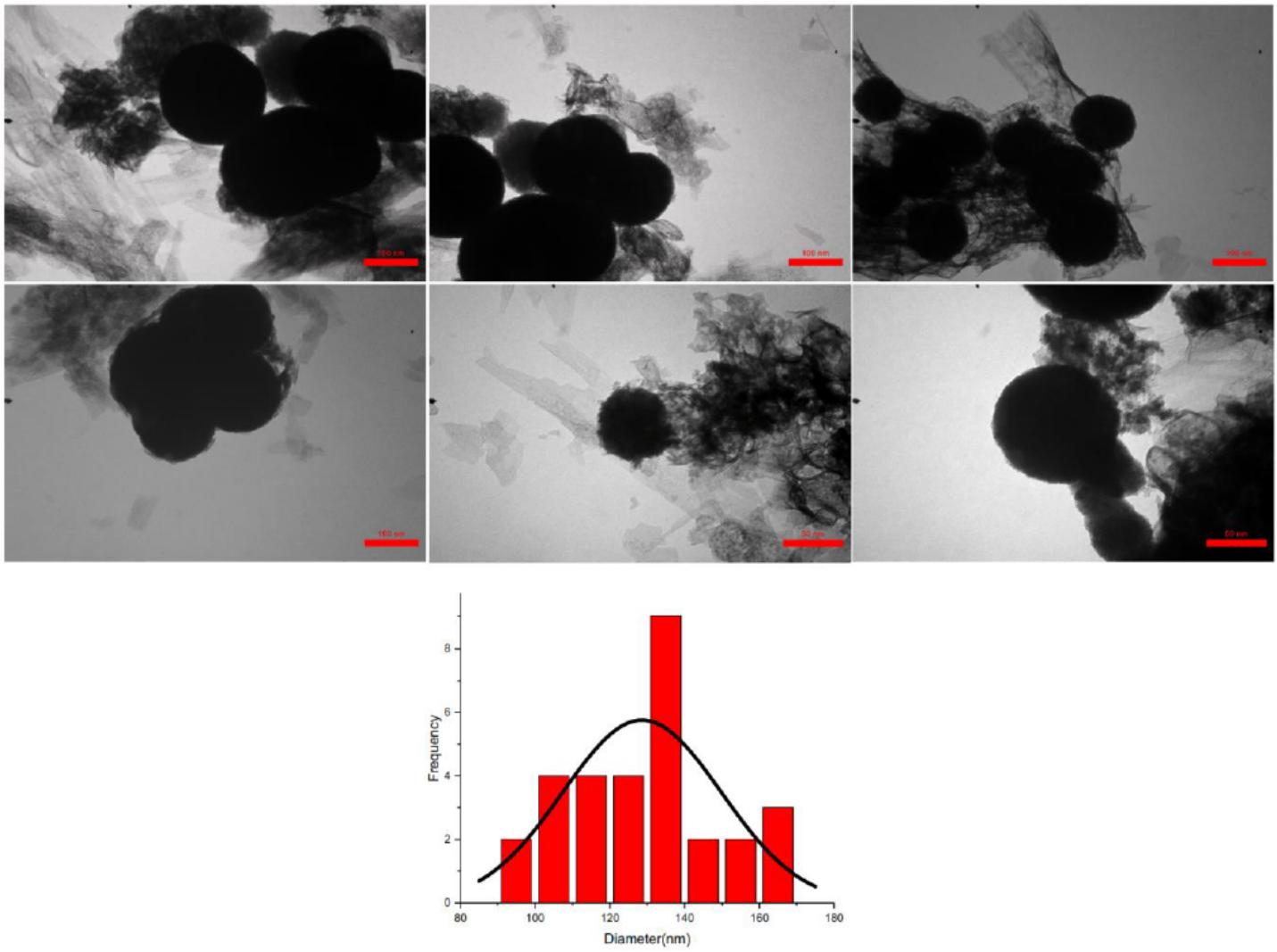

Figure 7

TEM images and particle size distribution histogram of Zn-MOF microspheres.

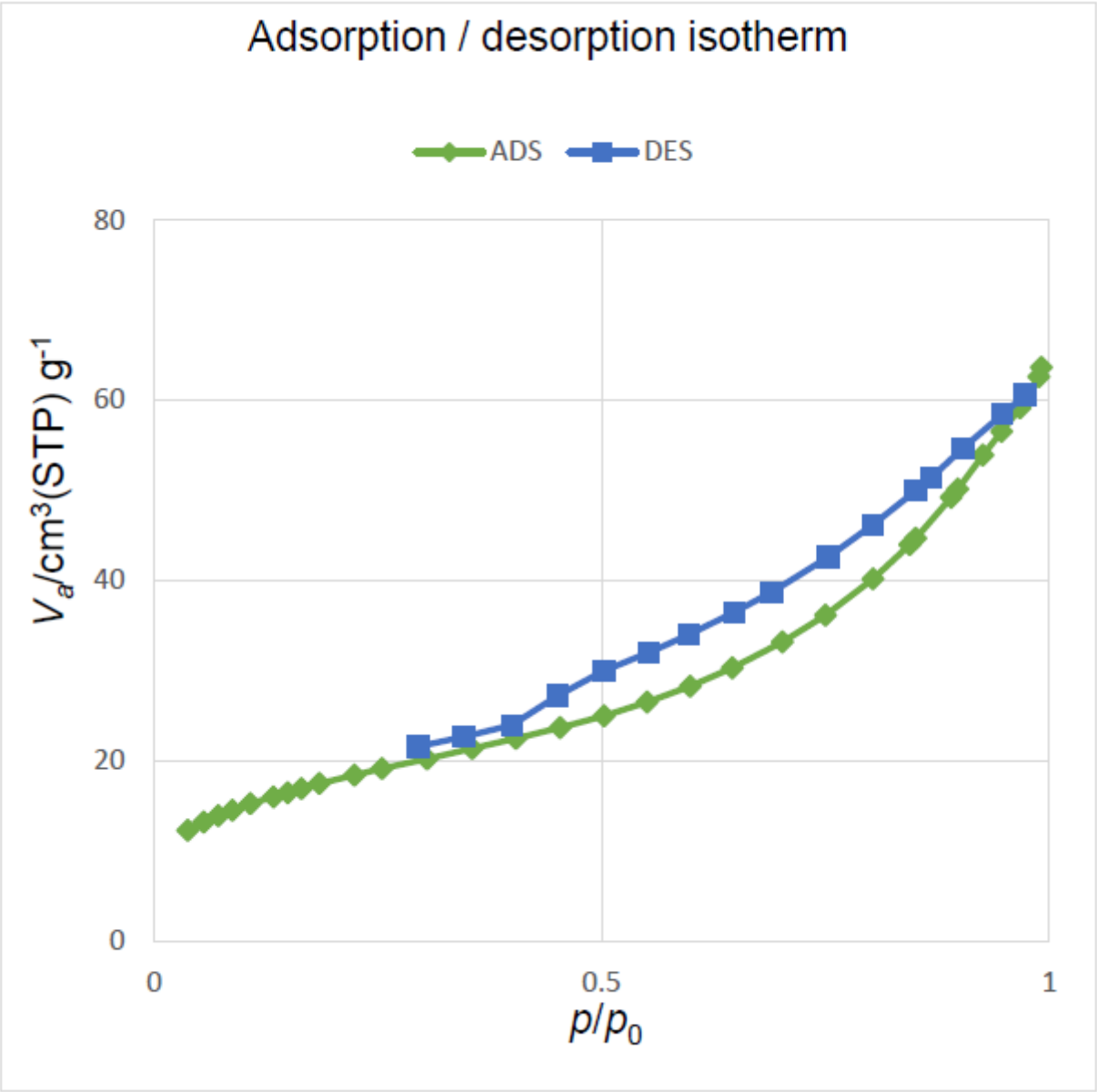

Figure 8

N2 adsorption/desorption isotherms of the nanoporous Zn-MOF microspheres.

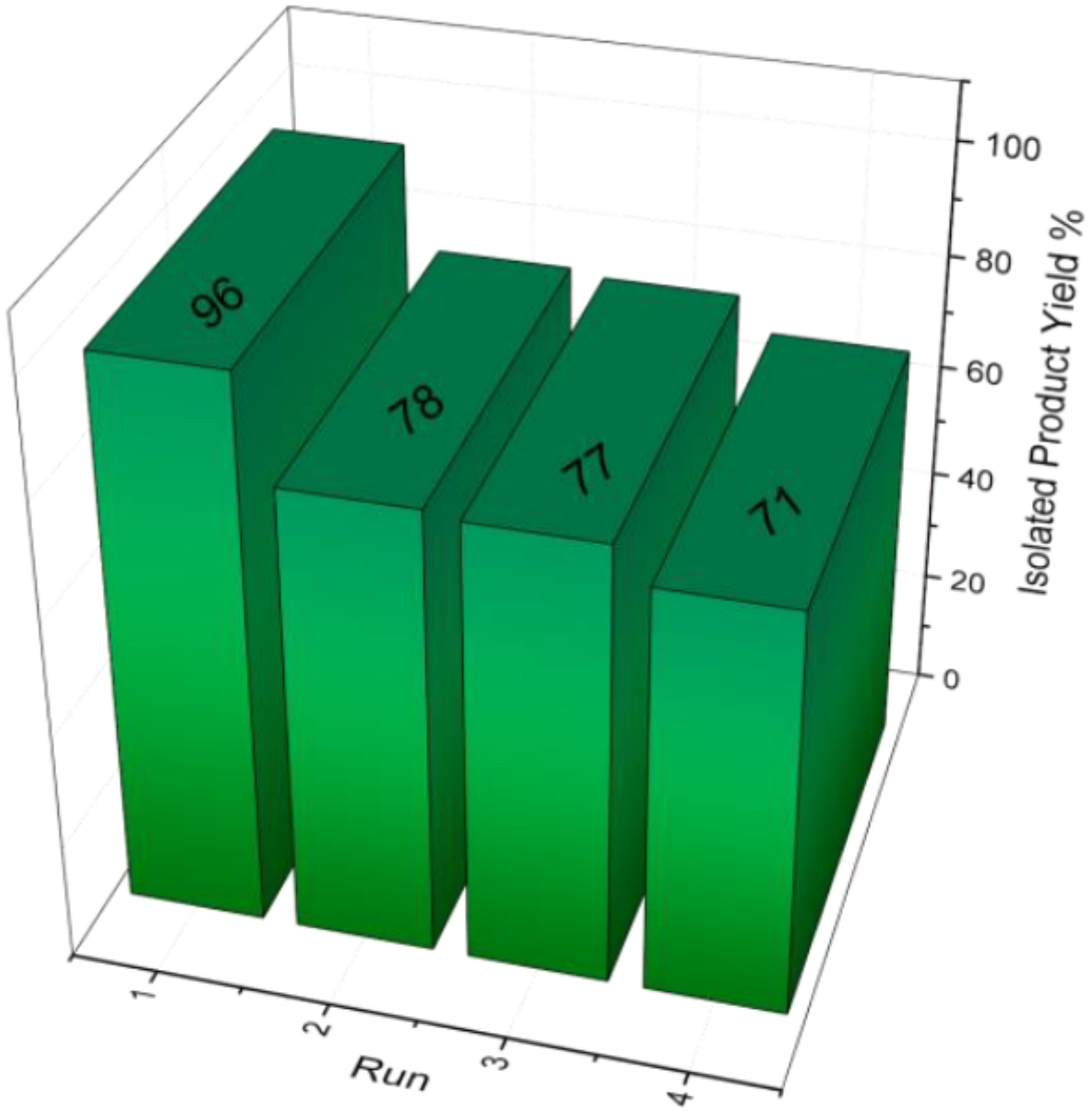

Figure 9

Recyclability of the nanoporous Zn-MOF microspheres.

Supplementary Files

This is a list of supplementary files associated with this preprint. Click to download.

- SupportingInformation.docx
- Scheme1.png

- Scheme2.png